Automatic Saturation Correction for Dynamic Range Management Algorithms

Alessandro Artusi[a,*], Tania Pouli[b], Francesco Banterle[c], Ahmet Oğuz Akyüz[d]

[a] *KIOS Center of Excellence University of Cyprus, Cyprus*

[b] *Technicolor, Cesson-Sévigné, France*

[c] *Visual Computing Laboratory, ISTI-CNR, Pisa, Italy*

[d] *Middle East Technical University, Ankara, Turkey*

Abstract

High dynamic range (HDR) images require tone reproduction to match the range of values to the capabilities of a display. For computational reasons and given the absence of fully calibrated imagery, rudimentary color reproduction is often added as a post-processing step rather than integrated into tone reproduction algorithms. In the general case, this currently requires manual parameter tuning, and can be automated only for some global tone reproduction operators by inferring parameters from the tone curve. We present a novel and fully automatic saturation correction technique, suitable for any tone reproduction operator (including inverse tone reproduction), which exhibits fewer distortions in hue and luminance reproduction than the current state-of-the-art. We validated its comparative effectiveness through subjective experiments and objective metrics. Our experiments confirm that saturation correction significantly contributes toward the perceptually plausible color reproduction of tonemapped content and would, therefore, be useful in any color-critical application.

Keywords: `High Dynamic Range Imaging, Color Correction, Gamut Mapping, Tonemapping, Inverse/Reverse Tonemapping`

☆

*Corresponding author

Email address: `artusialessandro4@gmail.com` (Alessandro Artusi)

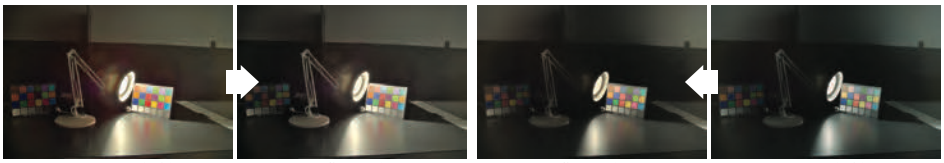

Figure 1: *The same HDR image was tonemapped with different operators (left - [1], right - [2]). The left tonemapped image is overly saturated, while the right image has reduced the saturation too far. With our method, both images are automatically corrected to have a similar appearance (source image from [3]).*

1. Introduction

Recent advances in both capture and display technologies allow images of a much wider dynamic range to be photographed, manipulated, and displayed; better capturing the light of natural scenes and giving artists unparalleled freedom. Although HDR standards and workflows are being defined and have begun to be adopted, they are not yet mainstream. As such, HDR technologies currently coexist with more prevalent consumer imaging pipelines [4]. HDR data often needs to be compressed for display on most current displays, a process known as tonemapping or tone reproduction. In contrast, existing low dynamic range (LDR) data may need to be expanded or reconstructed in order to fit the capabilities of emerging HDR display devices, a process known as inverse/reverse tonemapping (ITM) [5]. In both cases, the aim is to preserve the appearance and information content of an image as much as possible while ensuring that it can be displayed on the chosen display device. To achieve that, tonemapping and inverse tonemapping algorithms typically operate on the luminance of the image with little to no consideration for the color information present, leading to noticeable changes in the color appearance of the image, as shown in Figure 1.

Commonly, luminance-compressed images acquire an over-saturated appearance when only the luminance channel is processed [6, 7]. Image appearance models, which can be seen as tone reproduction operators with integrated color appearance management [2], are designed to reproduce color appearance, but they require calibrated images, precise knowledge of the scene in which the image was taken as well as measurements

of the viewing environment and the display device itself. This makes these algorithms very useful in color-critical applications, but their requirement for measurements coupled with high computational complexity due to spatially varying processing limits their general applicability.

Some solutions exist for correcting saturation mismatches after tonemapping [7]. This leads to a computationally efficient correction, although hue and luminance shifts may be introduced. Moreover, they require manual parameter selection which is strongly image and tone reproduction operator dependent. Recently, a subjective study was conducted for defining an automatic model to derive the parameters necessary for such corrections, but only allows parameters to be predicted when the tone compression or expansion function is global [6]. In this paper, we therefore, present an efficient and effective color post-processing technique with the aim to relieve the user from having to set parameters, while being applicable to any form of image processing, whether spatially varying or not. This has the additional benefit that our post-processing can be applied even if the input image was manually touched-up, including but not limited to manual dodging and burning. Our work offers the following contributions and advantages: (1) Our novel algorithm is based on recent advances in perceptually linear color-space and saturation computation. (2) Irrespective of the applied image processing technique or tonemapping operator, our algorithm is fully automatic and able to recover an accurate reconstruction of image saturation. (3) We take the gamut boundary of the output color space into consideration, leading to lower hue shifts and significantly lower luminance distortion. (4) We evaluate our algorithm by means of a subjective experiment and objective metrics, revealing that our algorithm reproduces saturation significantly better, as well as significantly reduces luminance distortions than the current state-of-the-art.

2. Hue and Saturation Correction

Tonemapping aims to compress the dynamic range of images and prepare them for display. Typically, this happens through a non-linear transformation of the luminance

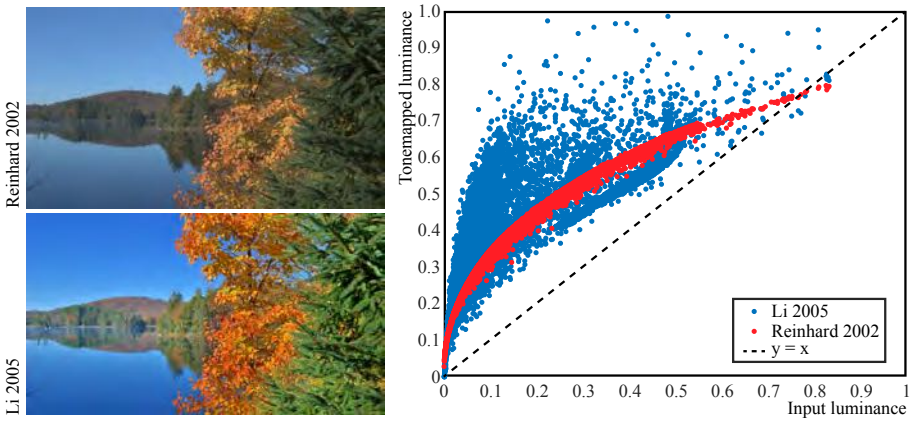

Figure 2: *Normalized input versus output luminance for two tonemapping operators. The parameters used are the one specified in their original work [8] and [1]. Note that each operator changes the relationship between input and output luminance in different ways leading to different types of saturation and hue shifts.*

channel. The aim of tonemapping is then two-fold; images need to be processed so that their absolute luminance range is compressed, but pixel relations also need to be altered to maximize visible detail, therefore changing the contrast in the image. Changes to contrast and luminance, however, often lead to changes in the appearance of colors in the image and specifically in their saturation and hue. Furthermore, different tonemapping algorithms alter luminance and contrast in vastly different ways (Figure 2), preventing a simple correction parameter to work for all cases. Thus, our algorithm is designed to correct the image's appearance while minimizing luminance and contrast modifications without requiring the user to set any parameter [9].

2.1. Algorithm Overview

The input to the algorithm consists of two images given in a linear RGB color space: the tone compressed image $\mathbf{M}_t$ and the original, unprocessed HDR image $\mathbf{M}_o$ as it contains the original saturation and hue values that we aim to reproduce. In case the input tonemapped image is gamma corrected, an inverse gamma correction is performed to linearize its RGB values. The goal of our algorithm is to modify $\mathbf{M}_t$ such that it matches $\mathbf{M}_o$ in terms of hue and saturation, while preserving luminance values from the tonemapped image $\mathbf{M}_t$. Note that matching the *appearance* of saturation requires

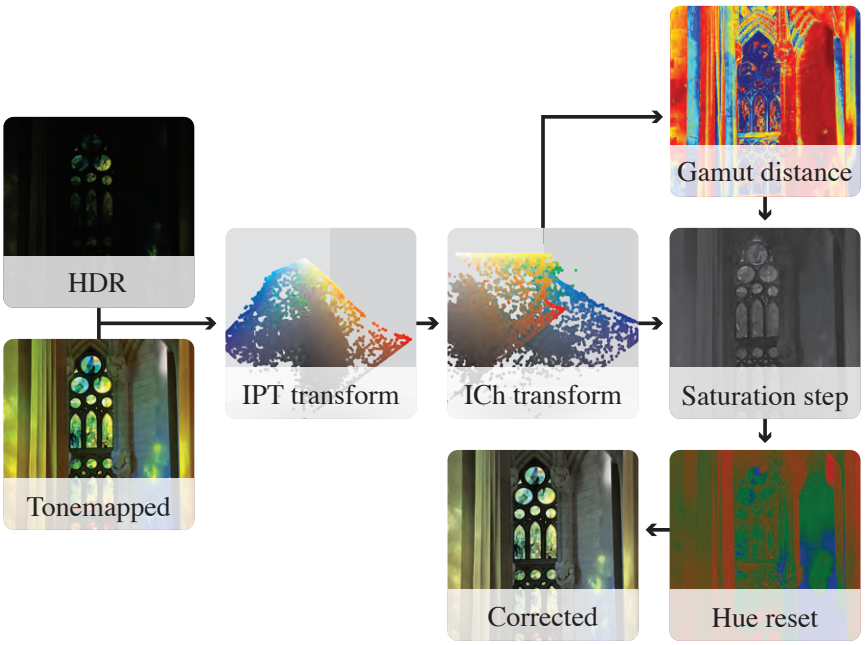

Figure 3: *The steps of our color management algorithm, here illustrated in the context of dynamic range compression.*

active non-linear management of saturation values to account for the Hunt effect [10]. Although HDR images are given in linear units, since in most cases accurate radiometric data is not available, their luminance values are inherently inaccurate. As such, we focus on contrast changes between the two input images and therefore normalize both $\mathbf{M}_t$ and $\mathbf{M}_o$ before converting them to the IPT color space, which has better hue uniformity than CIE $L^*a^*b^*$ and HSV color spaces [11]. Recently, a variant of the IPT space for HDR images, known as $hdr-IPT$ space, has been proposed. In this new space, the power function in IPT has been replaced with the Michaelis-Menten function to improve the behavior of the color space for very low and very high luminance levels [10]. We decided to not use this color space to avoid using different color spaces for tonemapped and HDR images.

As we need separate access to lightness, hue and colorfulness, we then convert to a cylindrical color space akin to CIE $L^*C^*h^*$. This space is based on IPT and therefore we refer to it as the ICh space, where I encodes lightness, C represents colorfulness

and h is a measure of hue. The lightness channel I is not further processed because this was the main purpose of the preceding tonemapping operator. The hue in the tonemapped image h_t is subsequently set to the hue h_o of the original image, restoring any hue distortions that may have arisen due to gamut clipping during tonemapping. The quantity that needs to be matched between the HDR and tonemapped images is saturation (s). However, the aforementioned cylindrical color space produces colorfulness (C). Saturation is defined as colorfulness relative to lightness, i.e. $s = C/I$. However, a recent proposal to define saturation as colorfulness relative to the full magnitude of the stimulus, i.e. $s = C/\sqrt{C^2 + I^2}$ [12], provides more accurate results for our application.

After the saturation is adjusted on a per-pixel basis, our adjustment is modulated to avoid creating out-of-gamut pixels. Finally, the corrected image is converted back to the RGB color space and gamma corrected as the final step. The workflow of our algorithm is illustrated in Figure 3 and discussed in detail in the following sections.

2.2. The IPT Color Space

Accurate color processing often benefits from the use of a perceptually linear and decorrelated color space. An obvious choice in this case would be the CIE $L^*a^*b^*$, as it aims to be perceptually uniform, meaning that the color difference between two pairs of colors with the same Euclidean distance between them in the CIE $L^*a^*b^*$ space will be perceived equally different. Although this is a useful property, images modified in the CIE $L^*a^*b^*$ may acquire hue shifts [11].

To address this particular shortcoming, an alternative color space known as IPT was proposed, where I encodes lightness information while the P and T channels (standing for *protan* and *tritan* responses) encode red-green and yellow-blue opponent dimensions respectively [11]. Like CIE $L^*a^*b^*$, it is defined as a transform from XYZ tristimulus values. The perceptual uniformity offered by CIE $L^*a^*b^*$ is preserved in IPT, but additionally changes in colorfulness do not induce hue shifts (see Figure 4), making it better suited for our purposes. The IPT space forms the foundation for our

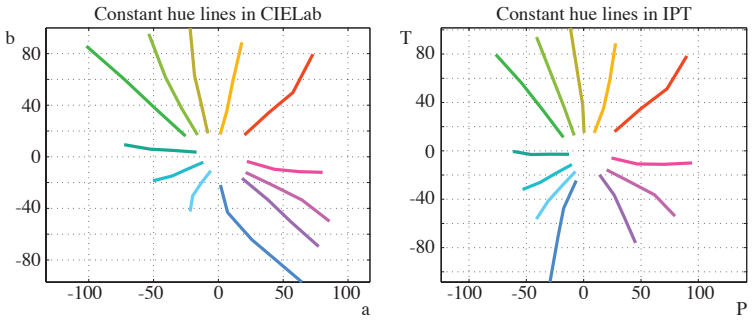

Figure 4: *Constant perceived hue lines plotted in the chromatic channels of CIE$L^*a^*b^*$ (a and b) and IPT (P and T). Straight lines indicate good hue-uniformity. Note that blue hues acquire significant shifts in the CIE $L^*a^*b^*$ color space, as shown by the curvature of the hue lines. Adapted from [13].*

algorithm. However, we wish to manipulate perceptual correlates of hue and saturation, and for this reason we convert from IPT space to a cylindrical version of IPT, which we term ICh, as explained next.

2.3. Appearance Correlates

To convert from IPT to a cylindrical color space ICh, we follow the standard procedure and leave the I channel unchanged while setting hue h and colorfulness C as described in [9]:

$$h = \tan^{-1}(P/T) \tag{1}$$

$$C = \sqrt{P^2 + T^2} \tag{2}$$

Saturation s is commonly computed as $s(C, I) = C/I$. Recently, however, an alternative formula was proposed that follows human perception more closely [12]:

$$s(C, I) = \frac{C}{\sqrt{C^2 + I^2}} \tag{3}$$

Note, however, that to our knowledge application of this formula in ICh is novel; its development was centered around CIE $L^*C^*h^*$. The merit of using this formulation is assessed in Section 3.1.

2.4. Saturation Correction

Since saturation for a given pixel depends both mathematically and perceptually on its lightness, it can be expected that after tonemapping an image, its saturation values will be changed. Most tonemapping operators modify only luminance and leave chromatic information unchanged, which inevitably alters the relation between lightness and saturation in the image, therefore leading to an over-saturated appearance. Tonemapping typically maps luminance values in a non-linear manner. As a result, although the absolute luminance levels of the tonemapped image are likely to be lower than the original HDR scene if displayed on a conventional monitor, the relative luminance of many pixels will be increased compared to their surrounding pixels. According to the Hunt effect, these pixels will then appear even more saturated, requiring additional correction. Noting that we have already normalized both tonemapped and HDR images before converting to ICh, to account for the Hunt effect, we begin by scaling colorfulness according to the relative lightness of the original HDR and tonemapped images:

$$C_t' = \frac{I_o}{I_t} C_t \tag{4}$$

Then, using (3), we compute the ratio r between the saturation of the original and tonemapped image, albeit that we compute the latter using C_t', i.e. after accounting for the Hunt effect:

$$r = \frac{s(C_o, I_o)}{s(C_t', I_t)} \tag{5}$$

This ratio is then applied to colorfulness C_t' as a second factor to find the colorfulness appropriate for the tonemapped image:

$$C_c = r\ C_t' = r \frac{I_o}{I_t} C_t \tag{6}$$

For convenience, in the following, we will refer to the full adjustment factor as:

$$r' = r \frac{I_o}{I_t} \tag{7}$$

Dependent on the used tone curve, the colorfulness of some pixels may increase while for others it may decrease. This may even happen in the same scene, so that light

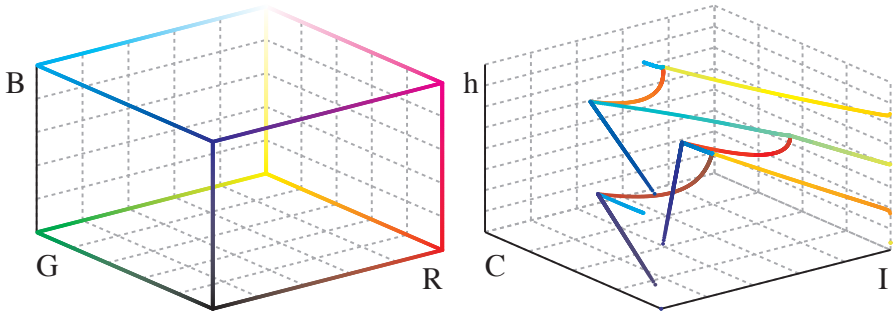

a. RGB gamut boundaries

b. RGB gamut boundaries plotted in ICh

Figure 5: *The RGB gamut boundary and the corresponding boundaries when plotted in ICh.*

pixels may gain in colorfulness, while dark pixels may lose colorfulness. This is a desired effect, but it does mean that light pixels may be moved toward and over the gamut boundary as a result of applying a scale factor that is larger than 1. To prevent this, it is possible to readjust the value of r' prior to applying it to the colorfulness of the tonemapped image. This is discussed in the following section. Finally, we reset the hue by copying values from the HDR image ($h_c = h_o$). Together with the corrected colorfulness C_c, it is combined with the lightness channel of the tonemapped image $I_c = I_t$ to produce the final corrected result, which can then be converted back to RGB and then gamma corrected for display purposes.

It should be noted that in this work we assume that both the input and the output target encoding —both in terms of color space and non-linearity—is BT.709 [14]. If a different output encoding is necessary, e.g. BT.2020 [15], which may be the case when inverse tonemapping content towards HDR, we propose that the transformation towards the desired encoding is performed after our processing, using the linear output of our algorithm.

2.5. Gamut Correction

When pixels in the tonemapped image $\mathbf{M}_t$ are near or on the gamut boundary, increases in colorfulness may lead to undesirable hue and luminance changes in the resulting

image due to gamut clipping in the conversion from ICh to RGB. Several gamut mapping techniques have been proposed, to solve this problem in the past[16]. These techniques have been mainly developed to overcome the limited mismatch between color gamuts, i.e., LDR image and display. Only recently techniques dealing with HDR content are starting to appear [17]. However, the aim of our gamut correction is two folds. The first is to perform this operation on the LDR content. The latter is to have a computationally efficient solution that does not add unacceptable extra overhead on the color correction algorithm, while maintaining acceptable quality.

To reduce the occurrence of such clipping, we developed a further adjustment to the colorfulness correction r'. The conversion between RGB and ICh is non-linear, and as such there is no easy way to determine what the maximum colorfulness is given a specific lightness level I and hue h. This can be seen in Figure 5 where we have plotted the vertices of an RGB cube before and after transforming to ICh. Although there may be analytic or sample-based solutions to describe the corresponding ICh gamut boundary, or distance metrics in complex volumes could be devised, these are not computationally efficient and would add a disproportionate cost to the main algorithm. Therefore, we propose a simplified and approximate algorithm to determine how far a given color is removed from the gamut boundary. Figure 5 shows that the RGB gamut is by definition cubic, and in our case it is located within the unit volume. Therefore, we compute the shortest distance of each pixel in the tonemapped image to the gamut boundary in RGB space:

$$\mathbf{d} = 2\ \min(\mathbf{M}_t, 1 - \mathbf{M}_t) \tag{8}$$

$$d = \min(\mathbf{d}_r, \mathbf{d}_g, \mathbf{d}_b) \tag{9}$$

where the factor of 2 normalizes the distance d. The approximation we make is that we assume the distance to the gamut boundary in RGB space to correlate with the distance to the gamut boundary in ICh space. We, therefore, use distance d to directly adjust the colorfulness scale factor.

We achieve out-of-gamut detection by converting a copy of the tonemapped image after the hue reset back to RGB and compute d based on that. Wherever hue reset

has created gamut related problems, we will have a value of d less than 0, meaning that at least one of the color components have gone out of the $[0, 1]$ range. We now have a choice as to whether we would accept a hue shift or sub-optimal saturation for these out-of-gamut pixels. We could reduce colorfulness until these pixels become representable in the output RGB gamut, thereby minimizing hue shifts. On the other hand, we could accept these hue shifts and keep our saturation processing as accurate as possible. Either approach would be viable. However, to demonstrate the utility of our algorithm, we have chosen for the latter by simply clamping negative values of d to 0. On the basis of d, we can now adjust our correction factor if it were to move pixels too close to the gamut boundary, or beyond. Rather than hard clipping, it is often desirable to gently reduce the processing for pixels near the gamut boundary. We have found that a straightforward rational function allows us to effect such a gentle roll-off:

$$d' = \frac{d}{d + 0.01} \tag{10}$$

The steepness of the roll-off is controlled by the constant 0.01, a parameter that was determined empirically. Note that this choice of this parameter is not critical, so that changes to this parameter value would not unduly affect the results. The contrast adjustment then becomes:

$$C_c = \begin{cases} C_t \; r' & r' \leq 1 \\ C_t \; (d'r' + (1 - d')) & r' > 1 \end{cases} \tag{11}$$

This function effectively produces a non-linear interpolation between the desired adjustment factor and a factor of 1 when near the gamut boundary.

As mentioned previously, in this work, we consider that the input content is encoded in the BT.709 gamut, and in this gamut correction step, we aim to preserve it. If the target output gamut is larger, e.g. BT.2020, to compute the distance in Equation (8), we first need to transform the image M_t from BT.709 to the larger color space, passing by XYZ, and according to the transformations described in the respective standards. After this conversion, the gamut boundaries will represent the larger gamut, and therefore the distance d will be adjusted accordingly.

3. Evaluation

To assess the performance of our algorithm, we compressed the dynamic range of many challenging scenes with different tonemapping operators. We then processed the results with our color correction method and compared our results against both the automatic and manual versions of Schlick's and Mantiuk's algorithms[6, 7]. Since we assume that the color correction method is applied as a post-process and therefore has no direct access to the tonemapping algorithm, for Schlick and Mantiuk's techniques we estimate the tone curve from the image pair directly so that their parameters can be directly estimated.

In the following, we begin by showing in Section 3.1 the merit of several design decisions taken during the development of our algorithm. In Section 3.2 we show side-by-side comparisons with existing techniques as well as usage scenarios. Then, in Section 3.3 we assess and compare lightness and hue reproduction, which can be measured objectively. This is followed by an evaluation for the case of ITM in Section 3.4. Finally, the comparative performance of saturation reproduction is assessed with a psychophysical experiment, which is discussed in Section 3.5.

3.1. Evaluation of Design Decisions

In this paper, we argue that the choice of color space is critical to the success of our method. An obvious choice for color processing would be CIE $L^*a^*b^*$. However, consistent with the literature [11], we found that it has relatively poor behavior, particularly in blue regions. This can be seen in Figure 6 where we have applied our color processing in both CIE $L^*C^*h^*$ (left), derived from CIE $L^*a^*b^*$, and ICh (right). Here, we have also applied two different formulations for saturation, the commonly used $s = C/I$ and the more recently proposed (Equation 3). We see that in CIE $L^*a^*b^*$ with the standard saturation computation the sky takes on a purple tinge, an effect we have seen in other images as well. This is fixed by using the new saturation formula, but here the final result is too saturated. Using ICh space no undue color shifts are present in Figure 6, but we observe that here the standard saturation formula

Figure 6: *Comparisons between different variants of our algorithm, in particular comparing performance in CIE $L^*C^*h^*$ derived from CIE $L^*a^*b^*$ against ICh, paired with two different saturation formulations, namely $s = C/I$ and $s = C/\sqrt{C^2 + I^2}$ (substitute L for I in CIE $L^*a^*b^*$).*

C/I leaves the image somewhat too desaturated. These effects are seen to a greater or lesser extent in many images. We have therefore chosen to do our processing in ICh space, using the more recent saturation computation, as explained in Section 2.

3.2. Results and Comparisons

The algorithm was implemented in MATLAB, running on an Apple Macbook Pro with an Intel Core 2 Duo processor running at 2.3 GHz. Although our current implementation is not optimized for performance, typical examples tested at resolutions of around 1 MP were processed in approximately 5 seconds. More than 90% of that time was spent on color space conversions. The tonemapping operators' parameter values used in the evaluation, are the ones specified in their original papers. Our method corrects the saturation in the image on a per-pixel basis. This ensures that even extreme changes in saturation due to tonemapping or any other manual or automatic image processing

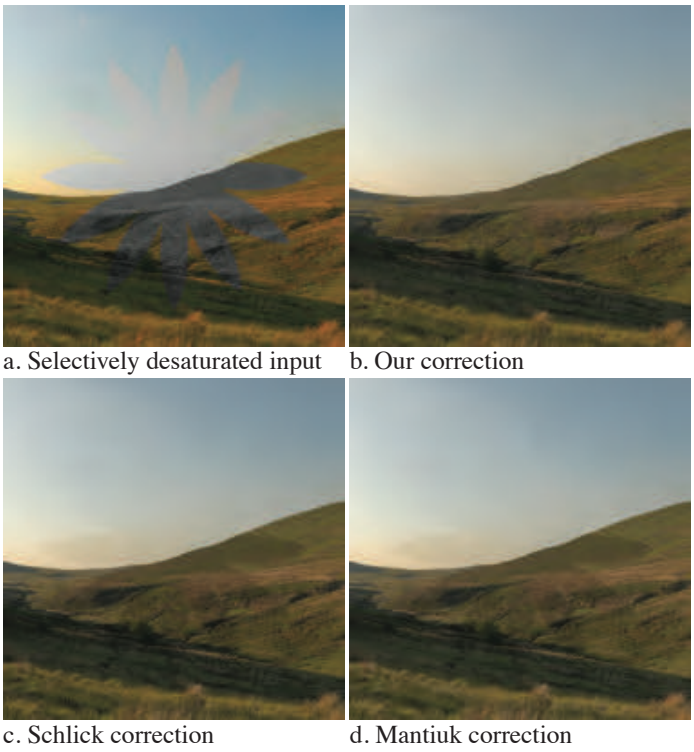

a. Selectively desaturated input b. Our correction

c. Schlick correction d. Mantiuk correction

Figure 7: *Typically, artists can use masks to control the contrast, saturation and other parameters locally in the image. The input image (a) was manually adjusted using a mask to selectively desaturate the logo, and post-processed with our algorithm (b) as well as Schlick's (c) and Mantiuk et al.'s [6] (d) corrections.*

can be corrected. Figure 7 demonstrates this with an example where the image is selectively desaturated using a mask. Although most of the image is overly saturated, a region in the shape of the logo is almost achromatic. The mask in this case has only affected saturation and not the luminance or contrast. Our approach corrects the colors in the image such that the desaturated logo becomes almost invisible after our correction.

Note that if both the HDR and the tonemapped images are individually normalized, the tone reproduction process does not universally reduce the image's contrast. Instead, some pixels are reduced in level, whereas others are increased. As a result, some pixels require a commensurate decrease in saturation, while others need their saturation to be increased. Figure 8 shows that the effect of our method is that materials can be correctly reproduced, irrespective of tone reproduction operator. The gold leaf on the

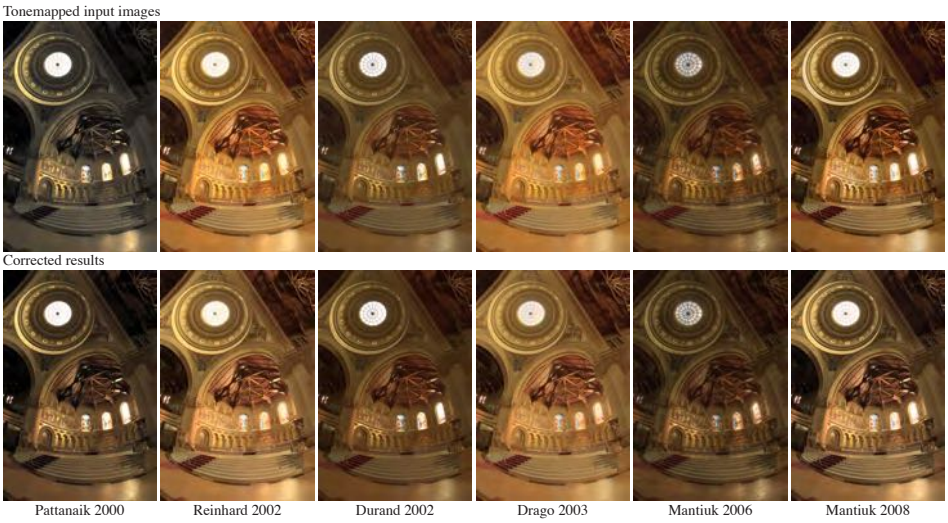

Figure 8: *The Memorial image was tonemapped using six different tone reproduction operators. The saturation was then corrected using our method, as well as Schlick's and Mantiuk's algorithms with parameter automation enabled [6]. Our method desaturates darker areas in the image more, following color perception, while lighter areas are preserved or even enhanced. As a consequence, the gold plating on the wall (inset) maintains a gold appearance in our results.*

wall still appears as gold for instance; an effect that is difficult to reproduce with other methods that tend to create more washed-out colors.

Figure 9 demonstrates that existing methods tend to desaturate parts of the image that are both light and saturated, turning the yellow sign and the shop interior white in the top images, and the sky gray in the bottom images. This effect is more pronounced with Li et al.'s operator [1] than with the photographic operator [8].

3.3. Luminance and Hue Differences

Ideally, saturation correction aimed at tone reproduction should alter the saturation or colorfulness of the image without affecting the luminance or hues. Specifically, the hues of the original input image should be preserved throughout the process, while the luminance and contrast information should be defined by the tonemapping process applied. To assess whether our algorithm achieves that, we have evaluated our results using color difference metrics.

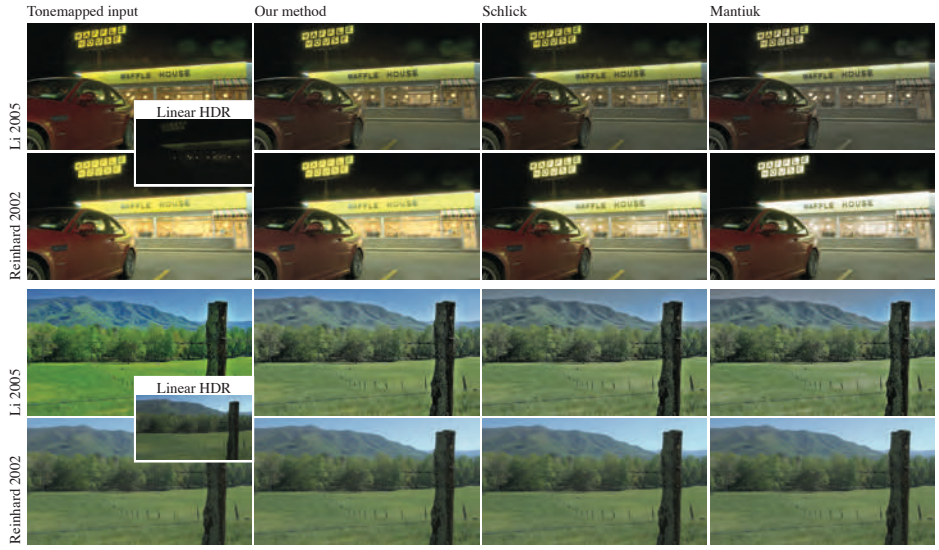

Figure 9: *Comparisons between our new algorithm and Schlick and Mantiuk's corrections.*

Typically, color differences are computed by simultaneously considering both luminance and chromatic information. In our case, a metric capable of separating luminance, saturation and hue is necessary as we are only interested in preserving two of these appearance correlates. Further, we compare hue information relative to the input HDR image, while luminance information is evaluated relative to the tone mapped image.

Although, commonly, color difference measurements are performed in the CIE $L^*a^*b^*$ color space, it is known that CIE $L^*a^*b^*$ is not hue-linear across all hues [11], making this space not ideal as a basis for measuring hue differences. The IPT color space addresses some of the limitations of CIE $L^*a^*b^*$, but to further optimize the space for computing color differences, an adjusted $I'P'T'$ color space was developed by Shen et al. [18]. This space is scaled and rotated with respect to IPT such that color differences are directly comparable with other color difference metrics, while preserving

hue linearity. It is computed from IPT coordinates as follows:

$$\begin{bmatrix} I' \\ P' \\ T' \end{bmatrix} = \begin{bmatrix} 100.0 & 0.0 & 0.0 \\ 0.0 & 144.9 & -2.1 \\ 0.0 & -39.1 & 85.5 \end{bmatrix} \begin{bmatrix} I \\ P \\ T \end{bmatrix} \tag{12}$$

In $I'P'T'$, a cylindrical space is then computed as discussed in Section 2, where lightness $\Delta I'$ and hue Δh differences can be computed. As hue is defined on a circle, we compute Δh for a given pair of hues h_t and h_c as follows:

$$\Delta h = \min(|h_t - h_c|, |\min(h_t, h_c) + 2\pi - \max(h_t, h_c)|) \tag{13}$$

Figure 10 shows aggregated results over a dataset of 99 HDR images, drawn from the HDR photographic survey [3], which were tonemapped twice; once with Li et al.'s algorithm [1] (right) and once with the photographic tone reproduction operator [8] (left). Lightness differences were evaluated against the tonemapped results in each case, while hue differences were evaluated against the input HDR image, to ensure that hue was preserved throughout the process. The GC and NGC abbreviations represent the gamut correction (Section 2.5) and no gamut correction cases, respectively.

We observe that lightness is significantly better reproduced in our method; slightly more so when the gamut boundary is taken into account. The performance improvement is particularly evident when the images are tonemapped with Li et al.'s method [1], a method known to require significant saturation post-processing. The photographic operator[1] [8] on average requires less severe saturation adjustment. Hue reproduction is also improved relative to the state-of-the-art, although less dramatically so. In the dataset of 99 images used in the experiment, we may find strong cases where the luminance shift of the state-of-the-art is well above the JND threshold of 2.3 [19], which is eliminated by our algorithm.

[1] In this paper we use the global version of this operator in all cases.

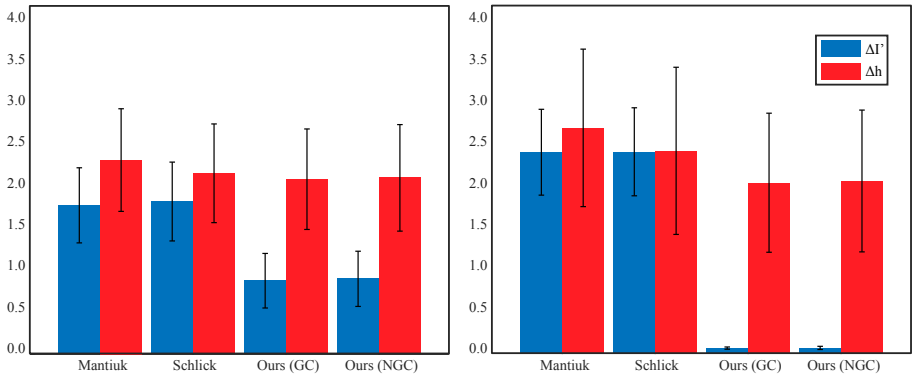

a. Reinhard 2002 b. Li 2005

Figure 10: *Left: Average $\Delta I'$ and Δh values between the tonemapped input and the corrected results using [7], our proposed approach, and [6] for* 99 *images taken from the HDR Photographic Survey [3]. Images were tonemapped with the photographic operator [8] and with Li et al.'s algorithm [1]. Error bars indicate a 95% confidence interval. The GC and NGC abbreviations represent the gamut correction (Section 2.5) and no gamut correction cases, respectively.*

3.4. Inverse Tonemapping

Our analysis so far has focused on the tone compression case. Nevertheless, the growing availability of commercial HDR displays has increased the need for color-managed solutions for expanding the dynamic range of existing LDR content. Recently, Bist et al. [20] study has shown that for gamma-expansion based ITM operators the ideal saturation parameter setting s is 1.25 when using the Mantiuk's luminance preserving formula. Our method is equally suitable for ITM applications [21]. We present a more holistic solution that irrespective of the ITM operator is fully automatic and able to recover an accurate reconstruction of image saturation. At the same time, we take the gamut boundary of the output color space into consideration, leading to lower hue shifts and significantly lower luminance distortion. ITM operators tend to create under-saturated results for the same reason that tonemapping operators tend to saturate too much. Figures 11 and 12 show that our algorithm is able to restore saturation in this case. Note that for visualization purposes each result was subsequently tonemapped with the photographic operator [8] .

In addition to visual comparisons, we evaluated the performance of the different cor-

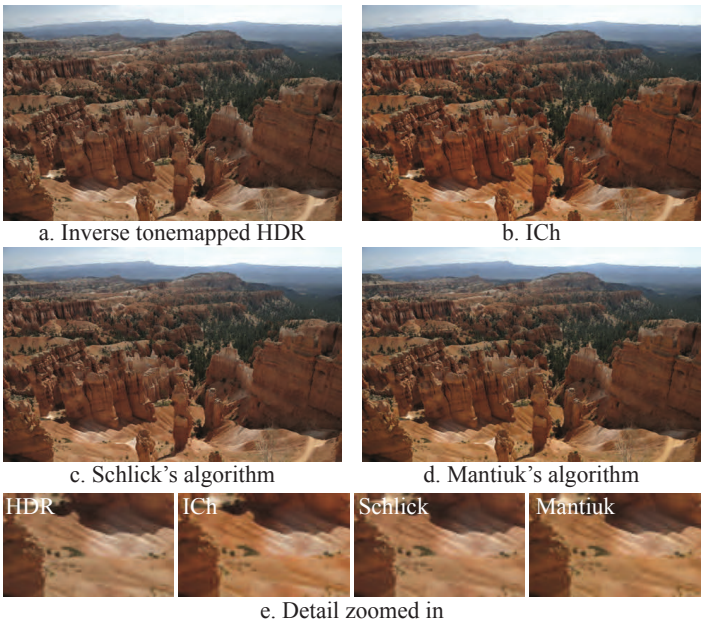

Figure 11: *An LDR image was passed through an IITM operator [21] (a) and then processed with our algorithm (b) and Schlick's (c) and Mantiuk et al.'s (d) algorithm.*

rection methods for several ITM methods by considering hue differences against the input LDR image and lightness differences against the ITM results. To provide comparable results to the TMO evaluation shown in Figure 10, LDR 'best exposures' were extracted from the 99 images of the HDR photographic survey [3], and were inverse tonemapped with the methods of Akyuz et al. [22], Kovaleski et al. [23], and Masia et al. [24]. Aggregated results are given in Figure 13 and example visualizations of difference maps are shown in Figure 14. The second row shows the lightness differences, while the last row shows the hue differences.

3.5. Psychophysical Evaluation

While luminance and hue performance can be assessed with suitably chosen color difference metrics, the aim of saturation correction algorithms is to alter saturation taking into account psychophysical phenomena. We have therefore chosen to compare and assess the performance of our algorithm relative to existing algorithm by means of a

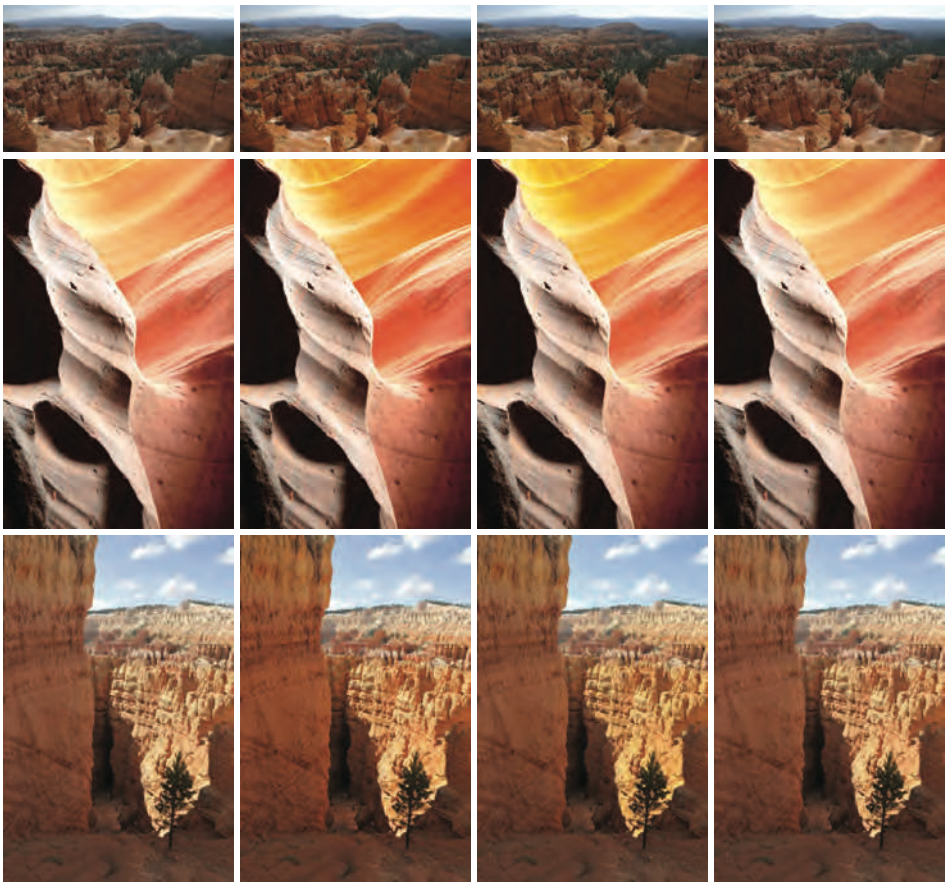

a. HDR from inverse tonemapping b. ICh post-processing c. Mantiuk post-processing d. Schlick post-processing

Figure 12: *Another example of applying our method to an ITM operator [21] (a) and then processed with our algorithm (b) and Schlick's (c) and Mantiuk et al.'s (d) algorithm.*

set of psychophysical experiments.

3.5.1. Experimental design

To assess the saturation performance, we designed a 2-alternative forced-choice experiment (2AFC) whereby two identically tonemapped images are post-processed with different saturation correction algorithms. These two images are shown side-by-side on the display, underneath the HDR input image as shown in the experiment set-up of Figure 16 To this end, we employed a SIM2 HDR47E S 4K HDR display device which

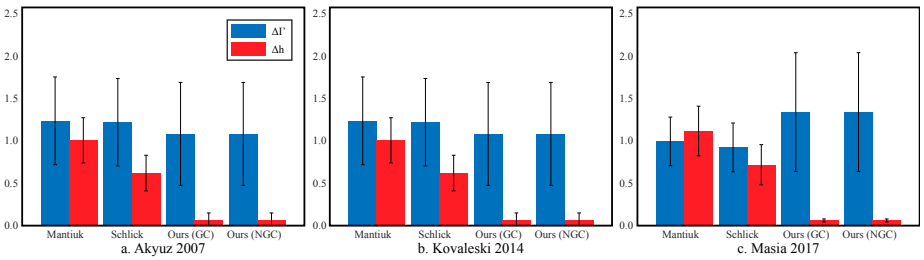

Figure 13: *Average $\Delta I'$ and Δh values between inverse tone mapped images and corrected results using [7], our proposed approach and [6] for 99 images. Our method was tested both with and without the gamut clipping step. Error bars indicate a 95% confidence interval.*

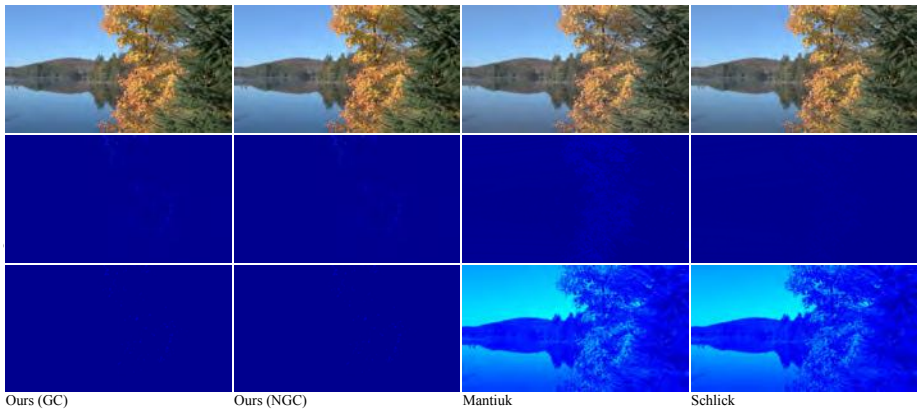

Figure 14: *Example results with different correction methods for ITM as well as corresponding lightness (second row) and hue differences (last row). ITM results for this example were obtained using the method of Akyuz et al. [22], and are shown after tonemapping for visualization.*

can emit up to $4000\ cd/m^2$. To allow prolonged stable and calibrated use, we used a peak luminance of no more than $2500\ cd/m^2$. The background of the stimuli was set to $18\ cd/m^2$ while the peak luminance for the tonemapped images was $100\ cd/m^2$. The left and right $7\ cm$ of the display were left unused as we have found luminance reproduction to be less accurate in those regions. The display was driven by an Apple Macbook Pro running Matlab using the Psychophysics toolbox extensions [25] and employing a custom OpenGL shader for driving the display in calibrated HDR mode. A set of 8 HDR images (stimuli) were drawn from the HDR Photographic Survey [3] shown in Figure 17. These HDR images were tonemapped with the global version of

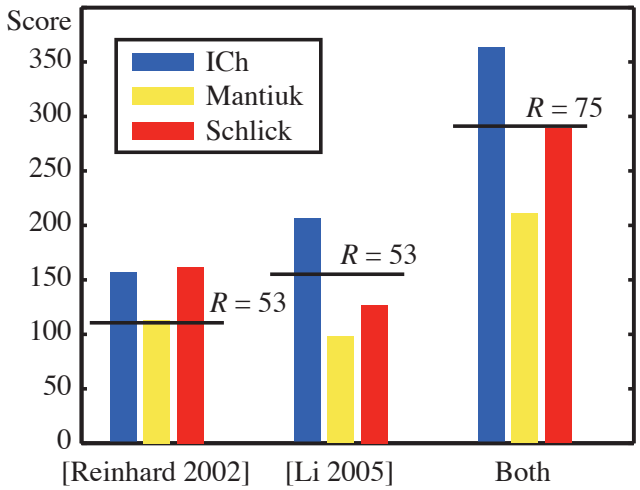

Figure 15: *Results from our experiment. The horizontal line indicates the difference with the longest bar in each group at which significance occurs.*

the photographic operator [8] and a spatially varying operator [1]. Subsequently, the images were post-processed with different saturation correction algorithms, dependent on the experiment (see below). A stimulus then consists of the HDR image, below which two differently post-processed images are shown. Tone mapping operators were varied between stimuli, but not within stimuli. In each trial, the participant was asked to select the image which matched saturation best to the HDR image. Before starting an experiment, participants were first shown written instructions, followed by a set of training screens consisting of patches with varying hues, lightness values and saturations. The purpose of these training screens, is to familiarize participants with the difference between saturation and other appearance phenomena. General feedback was solicited after the experiment, which lasted on average 20 minutes. The main experiments were preceded by two pilot studies to help configure the main experiment.

3.5.2. Pilot Studies

In the first pilot study, our algorithm with and without gamut correction is evaluated to determine which of these two versions performed best in terms of saturation reproduction. We found that both methods being selected virtually the same number of times.

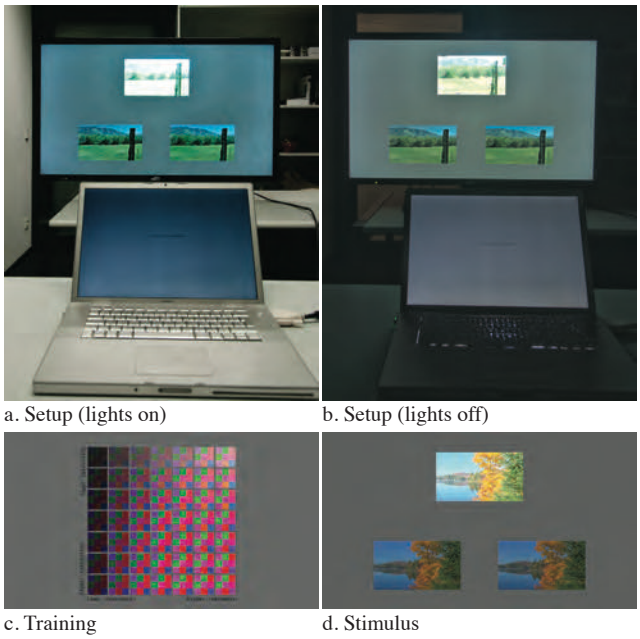

Figure 16: *Our experimental design: a. shown with room lights on for visualization purposes, b. without room lights demonstrating the conditions under which the experiment was run, c. one of the training screen and d. an example stimulus.*

However, as the gamut boundary solution, for specific cases, may provide better results we have chosen to include this variant in our experiment. In the second pilot study, the optimal parameters values for Schlick and Mantiuk are determined. In this study, a sequence of images with different parameters against the HDR image shown on the HDR display, were compared. The averaged values of the parameters are given in Table 1. It is interesting to note the wide range of values and their operator and image dependence, motivating the need for automation. These values were used to create stimuli for the experiment presented below.

3.5.3. Main experiment

The task for the main experiment is to match the impression of saturation between tonemapped color processed images and their HDR originals. Therefore, it is not a preference rating, but a match to sample task. Stimuli were created to compare our

Figure 17: *Images selected for our sebjective experiments, for visualization shown tonemapped with the photographic operator and post-processed with our algorithm. These images represent indoor, outdoor, landscape, photographs examples with a large variety of dynamic range.*

algorithm (which includes gamut boundary correction) with the automated version of Schlick and Mantiuk et al.'s algorithm using Li et al.'s [1] and Reinhard et al.'s [8] tone reproduction operators, leading to a total of 48 trials per participant to account for all paired comparisons. There were 18 participants in this experiment, who were between 23 and 53 years old, and all had normal or corrected-to-normal vision as well as normal color vision. We used a multiple comparison range test to determine if any pairwise difference was significant. This procedure, equivalent to Tukey's method used with ANOVA [26], is based on the range of the scores obtained by the color correction methods under examination. There is the possibility that circular triads can occur. This can be measured by calculating Kendall's coefficient of consistency ξ. We have calculated the ξ values per image and per tonemapping operator as shown in Table 2 . For the photographic operator we find an average coefficient of consistency of $\xi = 0.78 \pm 0.1$ (mean and standard deviation). For Li et al.'s operator we find $\xi = 0.85 \pm 0.08$. Thus, we have obtained overall high consistency, supporting the following findings. Significance tests were calculated on the differences between the scores of pairs of color correction methods [26]. These differences are considered significant if

Image	[Photographic 2002]		[Li 2005]	
	Schlick	Mantiuk	Schlick	Mantiuk
BarHarborSunrise	0.750	0.725	0.650	0.700
BloomingGorse2	0.875	0.900	0.800	0.900
LetchworthTeaTable1	0.675	0.725	0.725	0.700
LuxoDoubleChecker	0.775	0.825	0.750	0.775
MasonLake1	0.900	0.950	0.950	0.950
RedwoodSunset	0.650	0.700	0.650	0.625
SmokyTunnel	0.900	0.950	0.900	0.950

Table 1: *Manually selected values for parameter p in Schlick and Mantiuk's algorithms, per image and TMO.*

Images	[8]		[1]	
	ξ	u	ξ	u
1	0.88889	-0.90741	0.88889	-0.42593
2	0.77778	-0.57407	0.77778	-0.27778
3	1	-0.48148	0.77778	-0.48148
4	1	-0.81481	0.88889	-0.81481
5	0.77778	-0.77778	1	-0.68519
6	0.66667	-0.48148	0.88889	-0.40741
7	0.66667	-0.74074	0.66667	-0.83333
8	0.88889	-0.7037	0.88889	-0.37037

Table 2: *Coefficients of consistency ξ and agreement u per image and per tonemapping operator.*

they are greater than a critical value R which is computed as in [9]. Figure 15 shows the overall results of our experiment. When we assessed the overall performance, for each tonemapping operator, over all images, we found statistical significance for Li et al.'s operator at significance level $\alpha = 0.001$. The critical value is $R = 53$, given $u = 144$ for 18 participants $\times$ 8 images. In this case our method was selected significantly more often. This is visualized in Figure 15 where we have drawn a horizontal line at a height 53 below the maximum score, noting that the bars for Schlick and Mantiuk's methods do not cross this line. For the photographic operator, we found no statistically significant differences. We have observed that Li et al.'s operator on average requires stronger saturation correction than the photographic operator. It is therefore interesting

to see that especially in the case of Li et al.'s operator our saturation correction method performs well. Moreover, for the photographic operator our algorithm performs on par with the current state-of-the-art. We also computed scores for the two tonemapping operators combined. Here $R = 75$ as $u = 288$ (18 participants $\times$ 8 images $\times$ 2 tonemapping operators). Overall, our method was selected 364 times (289 times for Schlick's algorithm and 211 times for Mantiuk et al.'s method). This result, also shown in Figure 15, is therefore highly statistically significant ($\alpha = 0.001$). In essence, this means that our algorithm matches the impression of saturation between tonemapped, color corrected images and their HDR originals measurably better than the current state-of-the-art.

4. Conclusions

Tonemapping tends to be carried out on a luminance channel while leaving chromaticities unaffected. As the appearance of saturation depends on relative luminance levels, ideally saturation should co-vary with luminance when applying tonemapping operators. Nonetheless, it is possible to post-correct saturation mismatches given the input and the output images of a tonemapping algorithm. Based on recent insights into the design of perceptually linear color spaces as well as a recent formulation of saturation, our algorithm provides an effective solution for color post-processing of tonemapping operators as well as manually processed images. Our algorithm is shown to better preserve both lightness and hue information relative to the majority of different tonemapping and inverse tonemapping operators. As our solution is agnostic to the operator used, it can correct saturation after both local and global tonemapping, which is not currently possible with methods relying on estimating the slope of the tone curve. Although we do not explicitly address video content in this paper, our method can be further extended to handle video content in a temporally coherent manner, assuming that the tonemapping approach is temporally stable. This will be part of future work.

References

[1] Y. Li, L. Sharan, E. Adelson, Compressing and companding high dynamic range images with subband architectures, ACM Transactions on Graphics 24 (3) (2005) 836–844.

[2] E. Reinhard, T. Pouli, T. Kunkel, B. Long, A. Ballestad, G. Damberg, Calibrated image appearance reproduction, ACM Transactions on Graphics (Proceedings of SIGGRAPH Asia) 31 (6) (2012) article 201.

[3] M. D. Fairchild, The HDR photographic survey, in: Proceedings of the 15th IS&T/SID Color Imaging Conference, 2007, pp. 233–238.

[4] A. Artusi, F. Banterle, T. O. Aydin, D. Panozzo, O. Sorkine-Hournung, Image Content Retargeting: Maintaining Color, Tone, and Spatial Consistency, CRC Press, September 2016.

[5] F. Banterle, A. Artusi, K. Debattista, A. Chalmers, Advanced High Dynamic Range Imaging: Theory and Practice, AK Peters (CRC Press), Natick, MA, USA, 2011.

[6] R. Mantiuk, R. Mantiuk, A. Tomaszweska, W. Heidrich, Color correction for tone mapping, Computer Graphics Forum 28 (2) (2009) 193–202.

[7] C. Schlick, Quantization techniques for visualization of high dynamic range pictures, Proceedings of the 5th Eurographics Workshop on Rendering (1994) 7–18.

[8] E. Reinhard, M. Stark, P. Shirley, J. Ferwerda, Photographic tone reproduction for digital images, ACM Transactions on Graphics 21 (3) (2002) 267–276. doi:http://doi.acm.org/10.1145/566654.566575.

[9] T. Pouli, A. Artusi, F. Banterle, A. O. Akyuz, H.-P. Seidel, E. Reinhard, Color correction for tone reproduction, in: CIC21: Twenty-first Color and Imaging Conference, Society for Imaging Science and Technology (IS&T), 2013, pp. 215–220.

[10] M. D. Fairchild, Color Appearance Models 3rd ed., Cambridge University Press, 2013.

[11] F. Ebner, M. D. Fairchild, Development and testing of a color space (IPT) with improved hue uniformity, in: Sixth Color Imaging Conference: Color Science, Systems and Applications, 1998, pp. 8–13.

[12] E. Lübbe, Colours in the Mind - Colour Systems in Reality: A formula for colour saturation, Books on Demand GmbH, 2008.

[13] Y. Xue, Uniform color spaces based on CIECAM02 and IPT color difference equations, Ph.D. thesis, Rochester Institute of Technology (2008).

[14] I.-R. B. Recommendation, 709, Basic Parameter Values for the HDTV Standard for the Studio and for International Programme Exchange, now ITU-R BT 709.

[15] M. Sugawara, S.-Y. Choi, D. Wood, Ultra-high-definition television (rec. itu-r bt. 2020): A generational leap in the evolution of television [standards in a nutshell], IEEE Signal Processing Magazine 31 (3) (2014) 170–174.

[16] J. Morovic, Color Gamut Mapping, 1st Edition, The Wiley-IS&T Series in Imaging Science and Technology, 2008.

[17] E. Šikudova, T. Pouli, A. Artusi, A. Ahmet Oğuz, B. Francesco, E. Reinhard, Z. M. Mazlumoglu, A gamut mapping framework for color-accurate reproduction of HDR images, IEEE Transaction of Computer Graphics and Applications`doi:10.1109/MCG.2015.116`.

[18] S. Shen, Color difference formula and uniform color space modeling and evaluation, Ph.D. thesis, Rochester Institute of Technology (2009).

[19] O. A. Mahy M., VanEycken L., Evaluation of uniform color spaces developed after the adoption of cielab and cieluv, Color Research and Application 19 (1994) 105–121.

[20] C. Bist, R. Cozot, G. Madec, X. Ducloux, Special section on graphics interface 2016, Computers & Graphics 62 (Complete) (2017) 77–86. `doi:10.1016/j.cag.2016.12.006`.

[21] F. Banterle, P. Ledda, K. Debattista, A. Chalmers, Inverse tone mapping, in: GRAPHITE '06, 2006, pp. 349–356. doi:http://doi.acm.org/10.1145/1174429.1174489.

[22] A. O. Akyüz, R. Fleming, B. E. Riecke, E. Reinhard, H. H. Bülthoff, Do hdr displays support ldr content?: a psychophysical evaluation, ACM Trans. Graph. 26 (3) (2007) 38. doi:http://doi.acm.org/10.1145/1276377.1276425.

[23] R. P. Kovaleski, M. M. Oliveira, High-quality reverse tone mapping for a wide range of exposures, in: Graphics, Patterns and Images (SIBGRAPI), 2014 27th SIBGRAPI Conference on, IEEE, 2014, pp. 49–56.

[24] B. Masia, A. Serrano, D. Gutierrez, Dynamic range expansion based on image statistics, Multimedia Tools and Applications 76 (1) (2017) 631–648. doi:10.1007/s11042-015-3036-0.
URL https://doi.org/10.1007/s11042-015-3036-0

[25] D. H. Brainard, The Psychophysics toolbox, Spatial Vision 10 (1997) 433–436.

[26] H. A. David, The method of paired comparisons, in: Proceedings of the 5th Conference on the Design of Experiments in Army Research Developments and Testing, 1988, pp. 1–16.